Supplementary Material for

Effect of Daily Temperature Fluctuations on Virus Lifetime

Te Faye Yap,[1] Colter J. Decker,[1] Daniel J. Preston[1,*]

[1]Deptartment of Mechanical Engineering, Rice University, 6100 Main St., Houston, TX 77005

*To whom correspondence should be addressed
Phone: 713-348-4642
Email: djp@rice.edu

Other supplementary materials for this manuscript include the following:

Datasets S1 and S2

Supplementary Text

Numerical Analysis

Due to the dependence of temperature on time following the WAVE profile, the integral shown in Eq. **4** in the main text cannot be solved analytically. Euler's method is used to determine the concentration of virus at a given time for a given temperature profile, $T(t)$. Eq. **S1** through **S3** show the steps used to solve for the concentration after a given time step:

$$\int_{[C]_0}^{[C]} \frac{d[C]}{[C]} = \int_{t_0}^{t} -A \exp\left(-\frac{E_a}{RT(t)}\right) dt \qquad \text{[Eq. S1]}$$

$$\frac{[C]_{i+1} - [C]_i}{dt} = -A \exp\left(-\frac{E_a}{RT(t)}\right) [C]_i \qquad \text{[Eq. S2]}$$

$$[C]_{i+1} = -A \exp\left(-\frac{E_a}{RT(t)}\right) [C]_i \, dt + [C]_i \qquad \text{[Eq. S3]}$$

where i represents the number of time steps needed to determine the viable virus concentration. At $t = 0$, $i = 0$, corresponding to the initial virus concentration, $[C]_0$. The vertical axis in **Figure 2** in the main text is plotted in terms of an n-log reduction. This value is determined by taking the ratio between the concentration at a given time, $[C]$, and the initial concentration, $[C]_0$, in terms of orders of magnitude (the base-10 logarithm of the ratio):

$$n = log_{10} \frac{[C]}{[C]_0} \qquad \text{[Eq. S4]}$$

Quantitative Understanding of the Effects of DTR

We show that the virus concentration will always be lesser when taking into account the diurnal temperature range (DTR) compared to the case considering only mean temperature (**Figure S1(A)**). By evaluating the change in concentration over an infinitesimally small timestep (**Figure S1(B)**)**,** we can treat the local time-varying temperature profile as a step function, with ΔT representing an arbitrary temperature variation from the mean. To prove that the change in

concentration, Δ[*C*] (i.e., the final concentration minus the initial concentration) when accounting for DTR will be lesser (more negative) than when only considering the mean temperature over a given timestep, we start by assigning an inequality corresponding to our hypothesis:

$$\Delta[C]_{mean} > \Delta[C]_{DTR} \quad \text{[Eq. } \mathbf{S5}\text{]}$$

The Δ[*C*] is more negative for a greater magnitude of decrease in concentration, so the Δ[*C*] considering DTR will be less than the Δ[*C*] based on the mean temperature if temperature fluctuations result in a larger decrease in concentration. Based on the rate law for a first-order reaction, d[*C*]/dt = *C'*, which is also a function of temperature, *T*, the change in concentration is over an infinitesimally small timestep is:

$$\Delta[C] = C'(T)\Delta t \quad \text{[Eq. } \mathbf{S6}\text{]}$$

Substituting Eq. **S6** into Eq. **S5** and multiplying by the relevant timesteps shown in **Figure S1(B)** to determine the concentration, we obtain:

$$C'(T)(p+q)\Delta t > C'(T+p\Delta T)(q\Delta t) + C'(T-q\Delta T)(p\Delta t) \quad \text{[Eq. } \mathbf{S7}\text{]}$$

where *p* and *q* are numbers between 0 and 1 that sum to 1 (i.e., *p* + *q* = 1). We assign these *p* and *q* parameters to allow for a more general consideration of any asymmetric temperature profile for which the average of the temperature variations over a given timestep is equal to the mean temperature (**Figure S1(C)**). At the limiting case where *p* = 1 and *q* = 0 (or vice versa), the profile is equivalent to the mean temperature case.

Any arbitrary time-varying temperature profile *T*(*t*) can be constructed from a sum of many of these timesteps; therefore, by showing that this temperature profile with temperature fluctuations always results in a larger decrease in concentration than the mean temperature profile at every timestep, the result can be extended to any time-varying temperature profile *T*(*t*), including the temperature profile accounting for DTR in this work.

We take a second-order Taylor series expansion for a case with small temperature variations above and below the mean:

$$C'(T + p\Delta T) = C'(T) + \frac{dC'(T)}{dT}(p\Delta T) + \frac{1}{2}\frac{d^2C'(T)}{dT^2}(p\Delta T)^2 \quad \text{[Eq. } \mathbf{S8}\text{]}$$

$$C'(T - q\Delta T) = C'(T) - \frac{dC'(T)}{dT}(q\Delta T) + \frac{1}{2}\frac{d^2C'(T)}{dT^2}(q\Delta T)^2 \quad \text{[Eq. } \mathbf{S9}\text{]}$$

We substitute the second-order Taylor series expansion into Eq. **S7** to obtain:

$$C'(T)\Delta t > C'(T)\Delta t + \frac{d^2C'(T)}{dT^2}\frac{pq\Delta t\Delta T^2}{2} \quad \text{[Eq. } \mathbf{S10}\text{]}$$

When $\Delta T = 0$, we see that both sides of the inequality are equal, recovering the original form when only considering mean temperatures. In order for this inequality to hold true, the second term on the right-hand side must always be negative.

$$\frac{d^2C'(T)}{dT^2}\frac{pq\Delta t\Delta T^2}{2} < 0 \quad \text{[Eq. } \mathbf{S11}\text{]}$$

Since *p, q,* ΔT*,* and Δt are always positive, we focus on expanding the second order differential equation for *C*' by substituting the Arrhenius equation (Eq. S**18**):

$$\frac{d^2}{dT^2}\left(-Aexp\left(-\frac{E_a}{RT}\right)C_0\right) < 0 \quad \text{[Eq. } \mathbf{S12}\text{]}$$

Taking the first derivative with respect to temperature:

$$\frac{d}{dT}\left(-\frac{AC_0E_a}{R}exp\left(-\frac{E_a}{RT}\right)\frac{1}{T^2}\right) < 0 \quad \text{[Eq. } \mathbf{S13}\text{]}$$

Taking the second derivative with respect to temperature:

$$-\frac{AC_0E_a^2}{R^2}exp\left(-\frac{E_a}{RT}\right)\frac{1}{T^4} + \frac{2AC_0E_a}{R}exp\left(-\frac{E_a}{RT}\right)\frac{1}{T^3} < 0 \quad \text{[Eq. } \mathbf{S14}\text{]}$$

After simplifying Eq. **S14**, the criterion for $\Delta[C]_{mean} > \Delta[C]_{DTR}$ is:

$$\frac{1}{2}\frac{E_a}{RT} > 1 \quad \text{[Eq. } \mathbf{S15}\text{]}$$

In order to demonstrate that the inequality holds true for all relevant temperature conditions, we determined "worst-case scenario" values for the left-hand side of the inequality for the viruses studied in this work at the highest environmental temperature ever recorded on Earth (58 °C in El Azizia, Libya (Mildrexler et al., 2006)) to obtain conservative estimates (Table **S1**). We show that these values are always much greater than 1, demonstrating that fluctuating temperatures will always reduce virus lifetime compared to the corresponding mean temperature for the viruses studied here at any environmentally relevant conditions.

In fact, considering the case for Influenza A, the absolute temperature would need to be 7.5 times greater than the current characteristic environmental temperature (i.e., greater than ~2500 K) for the inequality to break down. Under all relevant environmental temperatures, the activation energy is much greater than the thermal energy. When comparing the Arrhenius equation with the Eyring equation, we also observe that the activation energy is approximately equal to the activation enthalpy, $\Delta H^{\ddagger}$, at environmental temperatures (i.e., the RT term is negligible in Eq. **S16**):

$$E_a = \Delta H^{\ddagger} + RT \qquad \text{[Eq. S16]}$$

We plotted the concentration of virus (Eq. **S3**) after a given timestep and compared the relative degree of inactivation when considering a fluctuating temperature profile to the case considering only the mean temperature to illustrate that the magnitude of change in concentration is always greater for the case of the fluctuating temperature profile (Eq. **S5**). The relative *n*-log reduction (where the value of *n* corresponds to the order-of-magnitude degree of inactivation) is defined as:

$$\frac{n_{DTR}}{n_{mean}} = \frac{log_{10}\frac{[C]_{DTR}}{[C]_i}}{log_{10}\frac{[C]_{mean}}{[C]_i}} \qquad \text{[Eq. S17]}$$

We plotted the relative *n*-log reduction against the value of *p* at a mean temperature of 20 °C for Δ*T* values of 5, 10, 15, and 20 °C (**Figure S1(D)**); the plot shows that considering fluctuations in temperature (such as DTR) will always serve to increase degree of inactivation, in turn resulting in a lower virus concentration. This trend illustrates that the inequality hypothesized in Eq. **S5** holds true. **Figure S1(D)** also shows that for a higher Δ*T*, a higher rate of inactivation can occur when temperature fluctuations above the mean are higher, but for a

shorter time period (i.e., $p > q$). At ΔT = 20 °C, we observe a fourfold increase in the relative n-log reduction of virus (i.e., one ten-thousandth of the initial concentration) as compared to the mean temperature case when $p \approx 0.8$, highlighting the exponential dependence of virus lifetime on temperature. From this quantitative approach, the duration and magnitude of temperature variations from the mean are shown to play a critical role in the degree of virus inactivation.

Temperature Profile

In **Figures 3** and **4** in the main text, the WAVE temperature profile is used to model daily environmental temperature fluctuations. In **Figure 3**, the sunrise time (**Dataset S2**) used to generate the temperature profile corresponds to each city shown. However, for the heat map shown in **Figure 4**, a more general temperature profile is used, in which the sunrise time is fixed at 0600 hours. Fixing the sunrise time has a negligible effect on the resulting computed virus lifetimes. The virus lifetimes in the five major cities studied in this work were determined using both city-specific sunrise times and an 0600 fixed sunrise time, with the average percentage difference for all cities between these two methods being 0.68% (**Figure S8**).

Influenza A Inactivation Data

Data on the inactivation of influenza virus (A/Puerto Rico/8/34/H1N1 strain) in terms of time required to achieve n-log reduction for a given temperature were obtained from Greatorex et al. (Greatorex et al., 2011). The data presented in their work corresponds to the inactivation of H1N1 on a fomite of stainless steel. The authors report experimental conditions with temperatures ranging from 17–21 °C; we used an intermediate value of 19 °C in our work. The relative humidity reported in their work was 23 – 24 %. The natural logarithm of 10^{-n} was plotted against time following the linearized rate law for a first-order reaction (Eq. **1**), and the time scale was converted to minutes according to convention. A linear fit for the data at 19 °C is presented in **Figure S2**. The resulting slope was used to determine the rate constant at this temperature, reported in **Table S2**.

We followed the same procedure to homogenize data on influenza virus (A/PR/8/34 H1N1 strain) reported by McDevitt et al. (McDevitt et al., 2010) for H1N1 on a fomite of stainless steel. Linear fits for data at 55, 60, and 65 °C at a relative humidity of 25% are presented in **Figures S3** through **S5**. The resulting slopes were used to determine the rate constants at these temperatures, reported in **Table S2**.

Influenza A Temperature-Dependent Inactivation

According to the rate law for a first-order reaction (Eq. **1**), the rate constant, k, can be determined for the inactivation of a virus at a given temperature, T, by applying a linear regression and calculating the slope, $k = -\Delta\ln([C])/\Delta t$. Each pair of k and T determined from the primary data is plotted according to the linearized Arrhenius equation (Eq. **S7**) and yields a linear relationship between $\ln(k)$ and $1/T$ (**Figure S6**). The slope and intercept of the linear fit correspond to the activation energy, E_a, and log of frequency factor, $\ln(A)$. The log of frequency factor, $\ln(A)$, is plotted against activation energy, E_a, for the viruses considered in this work; the linear correlation between $\ln(A)$ and E_a indicates that the viruses undergo a thermal denaturation process following the Meyer-Neldel rule, supporting our hypothesis that the viruses are inactivated due to the thermal denaturation of proteins that comprise each virion (**Figure S7**). The linear regression calculated in this work after including influenza A, [$\ln(A) = 0.394E_a - 5.63$], is similar to the linear regression tabulated in previous work for only coronaviruses (Yap et al., 2020), and is nearly identical to those calculated in two prior studies on the denaturation of tissues and cells, which report [$\ln(A) = 0.380E_a - 5.27$] (Qin et al., 2014) and [$\ln(A) = 0.383E_a - 5.95$] (Wright, 2003).

$$\ln(k) = -\frac{E_a}{RT} + \ln(A) \qquad \text{[Eq. S18]}$$

Temperature Data

The temperature data for the five most populous cities in the United States from January 1, 2020, to December 29, 2020, were obtained from the National Oceanic and Atmospheric Administration (NOAA) climate data online search database. Temperature data from weather stations located at the major airports in each city were used in this work, i.e., JFK International Airport (New York City), Los Angeles International Airport (Los Angeles), Chicago O'Hare International Airport (Chicago), George Bush Intercontinental Airport (Houston), and Phoenix Sky Harbor Airport (Phoenix). The complete temperature dataset is included as **Dataset S1**.

Sunrise Time Data

The sunrise times used to determine the time periods of the half-cosine functions in the temperature profiles for the five most populous cities in the United States from January 1, 2020, to December 29, 2020, were obtained from the National Oceanic and Atmospheric Administration

(NOAA) solar calculator. The complete dataset is included as **Dataset S2**; the highlighted rows and columns were adjusted for daylight saving time (note that Phoenix does not observe daylight saving time).

Fixed Sunrise Time (0600 hours) versus City-Specific Sunrise Time

The percentage difference in results when fixing the sunrise time at 0600 hours in the model versus assigning the actual sunrise time for each specific region is plotted in **Figure S9**. The low percentage difference (0.68% on average) allowed us to neglect the effect of region-specific sunrise time, and a fixed sunrise time at 0600 hours was used in the model to calculate the lifetimes displayed in the parametric sweep shown in **Figure 4** of the main text.

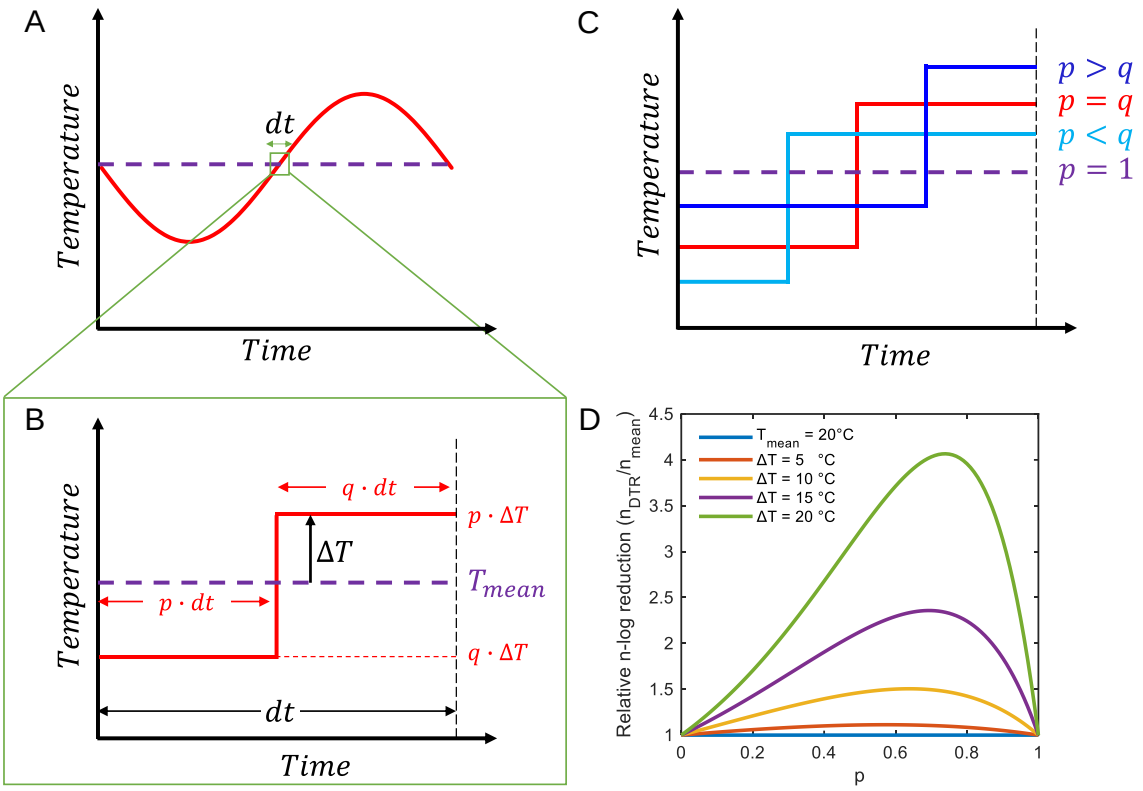

Fig. S1. (A) Sinusoidal temperature profile used to model temperature variations around the mean temperature. (B) Considering the temperature profile at a small timestep, the temperature profile can be approximated as a step function. The variables *p* and *q* are introduced to analyze cases where the temperature profile is not symmetric, but the average of this temperature profile is always equal to the mean temperature; *p* and *q* are positive numbers and $p + q = 1$. (C) Illustration of potential temperature profiles for different values of *p*. (D) The *n*-log reduction of virus inactivation when considering DTR, n_{DTR}, relative to the *n*-log reduction of virus when only considering mean temperatures, n_{mean}, against an array of *p* values varying from 0 to 1. The graph is plotted for a mean temperature of 20 °C and ΔT values of 5, 10, 15, and 20 °C to demonstrate the importance of considering DTR.

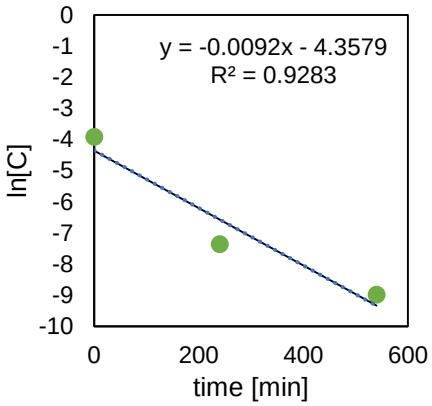

Fig. S2. Primary data from Greatorex et al. (Greatorex et al., 2011) for inactivation of H1N1 at 19 °C after converting the *n*-log reduction values from base-10 logarithm to natural log. We fit a line to the data to determine the rate constant at 19 °C.

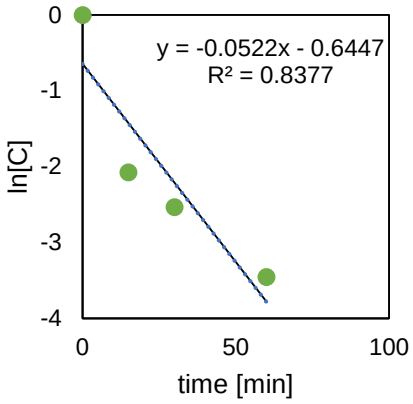

Fig. S3. Primary data from McDevitt et al. (McDevitt et al., 2010) for inactivation of H1N1 at 55 °C after converting the *n*-log reduction values from base-10 logarithm to natural log. We fit a line to the data to determine the rate constant at 55 °C.

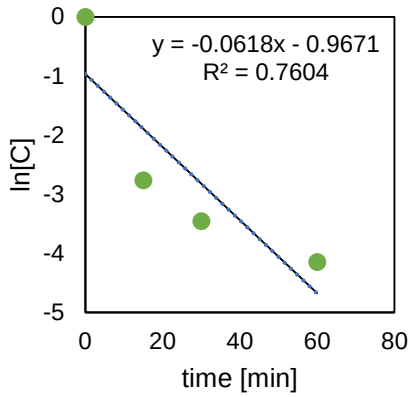

Fig. S4. Primary data from McDevitt et al. (McDevitt et al., 2010) for inactivation of H1N1 at 60 °C after converting the *n*-log reduction values from base-10 logarithm to natural log. We fit a line to the data to determine the rate constant at 60 °C.

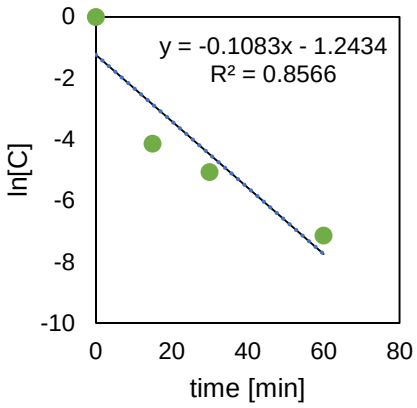

Fig. S5. Primary data from McDevitt et al. (McDevitt et al., 2010) for inactivation of H1N1 at 65 °C after converting the *n*-log reduction values from base-10 logarithm to natural log. We fit a line to the data to determine the rate constant at 65 °C.

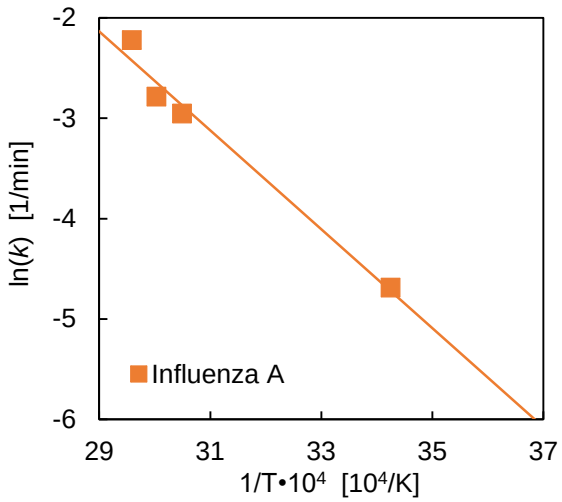

Fig. S6. From the Influenza A virus dataset, the rate constant, k, for a given temperature was found using linear regression according to Eq. **S5**. The slope and intercept of the linear fit correspond to the activation energy, E_a, and frequency factor, ln(A), for Influenza A.

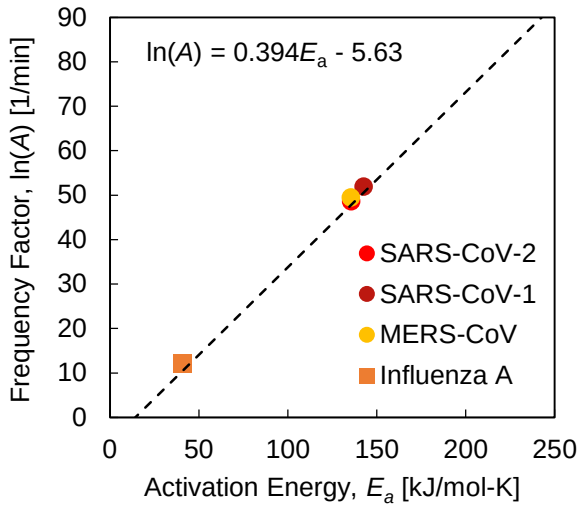

Fig. S7. Thermal inactivation parameters governing the inactivation behavior of SARS-CoV-2, SARS-CoV-1, MERS-CoV, and Influenza A. The frequency factor, ln(*A*), is plotted against the activation energy, E_a, according to the linearized Arrhenius equation.

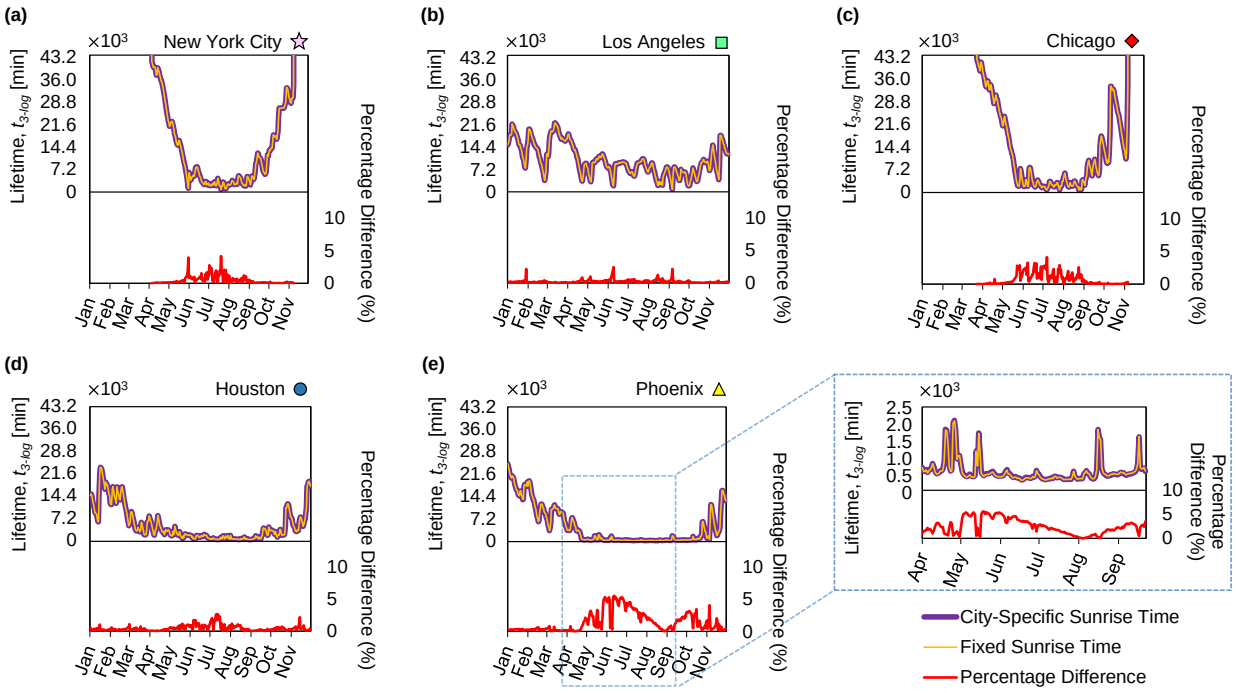

Fig. S8. The predicted lifetimes (7.2×10^3 min = 5 days) of SARS-CoV-2 for the months of January 2020 to November 2020, along with the percentage difference using city-specific versus fixed (0600 hours) sunrise times, are plotted for (a) New York City, (b) Los Angeles, (c) Chicago, (d) Houston, and (e) Phoenix. The average percentage difference between these methods for all cities is 0.68%. Phoenix experiences the highest percentage difference of 5.55%. The period with this high percentage difference, from April to September 2020, is magnified to show the difference in lifetimes, which is likely due to a higher rate of inactivation at the higher overall temperatures in Phoenix during these months, highlighting the importance of the period of time between sunrise and solar noon during high environmental temperatures.

Table S1: Values for the left-hand side of Eq. **S13** to show that the inequality is satisfied. Temperature was chosen as a conservative estimate for the maximum temperature attainable on Earth.

	Activation Energy, E_a [kJ/mol]	$E_a/2RT$ *(Eq.* ***S13)***
SARS-CoV-2	135.7	24.7 >> 1
SARS-CoV-1	142.6	25.9 >> 1
MERS-CoV	135.4	24.6 >> 1
Influenza A	41.0	7.5 >> 1

Table S2. Data for Influenza A obtained from Figures S2-5 and plotted in Figure S6 and data for SARS-CoV-2, SARS-CoV, and MERS-CoV from prior work (Yap et al., 2020).

Dataset	**SI Ref.**	**T [°C]**	**$1/T \cdot 10^4$ [10^4/K]**	**k = -d(ln[C])/dt [1/min]**	**ln(*k*) [1/min]**
Influenza A	(Greatorex et al., 2011)	19	34.25	0.0092	-4.689
Influenza A	(McDevitt et al., 2010)	55	30.49	0.0522	-2.953
Influenza A	(McDevitt et al., 2010)	60	30.03	0.0618	-2.784
Influenza A	(McDevitt et al., 2010)	65	29.59	0.1083	-2.223
SARS-CoV-2	(Chin et al., 2020)	4	36.10	0.0000597	-9.726
SARS-CoV-2	(Chin et al., 2020)	22	33.90	0.000696	-7.270
SARS-CoV-2	(van Doremalen et al., 2020)	22	33.90	0.00166	-6.401
SARS-CoV-2	(Chin et al., 2020)	37	32.36	0.00557	-5.190
SARS-CoV-2	(Chin et al., 2020)	56	30.39	0.724	-0.323
SARS-CoV-2	(Chin et al., 2020)	70	29.15	3.36	1.212
SARS-CoV-1	(van Doremalen et al., 2020)	22	33.90	0.00191	-6.261
SARS-CoV-1	(Darnell and Taylor, 2006)	56	30.40	0.9077	-0.097
SARS-CoV-1	(Darnell and Taylor, 2006)	65	29.59	2.869	1.054
MERS-CoV	(van Doremalen et al., 2013)	20	34.13	0.0027	-5.914
MERS-CoV	(Leclercq et al., 2014)	56	30.40	0.16	-0.999
MERS-CoV	(Leclercq et al., 2014)	65	29.59	3.62	2.121

Table S3. Experimental conditions at which E_a and ln(A) are determined for the viruses analyzed in this work.

Dataset	Ref.	T [°C]	Fomite	RH
SARS-CoV-2	(Chin et al., 2020)	4	Virus transport Medium	Not reported
SARS-CoV-2	(Chin et al., 2020)	22	Virus transport medium	Not reported
SARS-CoV-2	(van Doremalen et al., 2020)	22	Plastic	40%
SARS-CoV-2	(Chin et al., 2020)	37	Virus transport medium	Not reported
SARS-CoV-2	(Chin et al., 2020)	56	Virus transport medium	Not reported
SARS-CoV-2	(Chin et al., 2020)	70	Virus transport medium	Not reported
SARS-CoV-1	(van Doremalen et al., 2020)	22	Plastic	40%
SARS-CoV-1	(Darnell and Taylor, 2006)	56	Human serum	Not reported
SARS-CoV-1	(Darnell and Taylor, 2006)	65	Human serum	Not reported
MERS-CoV	(van Doremalen et al., 2013)	20	Plastic	40%
MERS-CoV	(Leclercq et al., 2014)	56	Modified Eagle's medium	Not reported
MERS-CoV	(Leclercq et al., 2014)	65	Modified Eagle's medium	Not reported
Influenza A	(Greatorex et al., 2011)	19	Stainless steel	23-24%
Influenza A	(McDevitt et al., 2010)	55	Stainless steel	25%
Influenza A	(McDevitt et al., 2010)	60	Stainless steel	25%
Influenza A	(McDevitt et al., 2010)	65	Stainless steel	25%

Supplementary Datasets

Dataset S1 (separate file). Temperature data corresponding to the five most populous cities in the United States.

Dataset S2 (separate file). Sunrise time data corresponding to the five most populous cities in the United States. Highlighted cells are adjusted for daylight saving time (note that Phoenix does not observe daylight saving time).

Supplementary Material References

Chin, A.W.H., Chu, J.T.S., Perera, M.R.A., Hui, K.P.Y., Yen, H.-L., Chan, M.C.W., Peiris, M., Poon, L.L.M., 2020. Stability of SARS-CoV-2 in different environmental conditions. The Lancet Microbe 1, e10. https://doi.org/10.1016/S2666-5247(20)30003-3

Darnell, M.E.R., Taylor, D.R., 2006. Evaluation of inactivation methods for severe acute respiratory syndrome coronavirus in noncellular blood products. Transfusion 46, 1770–1777. https://doi.org/10.1111/j.1537-2995.2006.00976.x

Greatorex, J.S., Digard, P., Curran, M.D., Moynihan, R., Wensley, H., Wreghitt, T., Varsani, H., Garcia, F., Enstone, J., Nguyen-Van-Tam, J.S., 2011. Survival of influenza A(H1N1) on materials found in households: Implications for infection control. PLoS One 6, 4–9. https://doi.org/10.1371/journal.pone.0027932

Leclercq, I., Batéjat, C., Burguière, A.M., Manuguerra, J.C., 2014. Heat inactivation of the Middle East respiratory syndrome coronavirus. Influenza Other Respi. Viruses. https://doi.org/10.1111/irv.12261

McDevitt, J., Rudnick, S., First, M., Spengler, J., 2010. Role of absolute humidity in the inactivation of influenza viruses on stainless steel surfaces at elevated temperatures. Appl. Environ. Microbiol. 76, 3943–3947. https://doi.org/10.1128/AEM.02674-09

Mildrexler, D.J., Zhao, M., Running, S.W., 2006. Where are the hottest spots on Earth? Eos (Washington. DC). 87, 461–467. https://doi.org/10.1029/2006EO430002

Qin, Z., Balasubramanian, S.K., Wolkers, W.F., Pearce, J.A., Bischof, J.C., 2014. Correlated Parameter Fit of Arrhenius Model for Thermal Denaturation of Proteins and Cells. Ann. Biomed. Eng. https://doi.org/10.1007/s10439-014-1100-y

van Doremalen, N., Bushmaker, T., Morris, D.H., Holbrook, M.G., Gamble, A., Williamson, B.N., Tamin, A., Harcourt, J.L., Thornburg, N.J., Gerber, S.I., Lloyd-Smith, J.O., de Wit, E., Munster, V.J., 2020. Aerosol and Surface Stability of SARS-CoV-2 as Compared with SARS-CoV-1. N. Engl. J. Med. https://doi.org/10.1056/NEJMc2004973

van Doremalen, N., Bushmaker, T., Munster, V.J., 2013. Stability of middle east respiratory syndrome coronavirus (MERS-CoV) under different environmental conditions. Eurosurveillance 18, 1–4. https://doi.org/10.2807/1560-7917.ES2013.18.38.20590

Wright, N.T., 2003. On a Relationship Between the Arrhenius Parameters from Thermal Damage Studies. J. Biomech. Eng. 125, 300–304. https://doi.org/10.1115/1.1553974

Yap, T.F., Liu, Z., Shveda, R.A., Preston, D.J., 2020. A predictive model of the temperature-dependent inactivation of coronaviruses. Appl. Phys. Lett. 117. https://doi.org/10.1063/5.0020782